



An oceanic cyclonic eddy on the lee side of Lanai Island, Hawai'i

Changming Dong,¹ Timothy Mavor,^{2,3} Francesco Nencioli,⁴ Songnian Jiang,⁴
Yusuke Uchiyama,¹ James C. McWilliams,¹ Tommy Dickey,⁴ Michael Ondrusek,²
Hongchun Zhang,⁵ and Dennis K. Clark²

Received 27 February 2009; revised 6 July 2009; accepted 9 July 2009; published 9 October 2009.

[1] A young cold core cyclonic eddy displaying a significant increase in surface chlorophyll was observed offshore Lanai Island, Hawai'i, where the Marine Optical Buoy (MOBY) is located. During one of its deployments, MOBY broke free from its mooring. In the course of its 3-day free drifting period, MOBY followed a cyclonic eddy, which is manifested by satellite remote sensing data, chlorophyll data from Moderate Resolution Imaging Spectroradiometer, and sea surface temperature (SST) from a Geostationary Operational Environmental Satellite. The time series of the SST show that the cold core eddy was in a formative stage. It existed as a stand-alone eddy for about 9 days before it merged with cold water south of Oahu Island. A high-resolution numerical model simulation reproduces similar eddies in terms of location, size, and intensity. An eddy detection algorithm is described and applied to locate and track the modeled eddies. The results demonstrate that mesoscale and submesoscale eddies are frequently generated on and pass through the lee side of Lanai Island and the statistical analysis quantifies the general features of eddies in the area.

Citation: Dong, C., T. Mavor, F. Nencioli, S. Jiang, Y. Uchiyama, J. C. McWilliams, T. Dickey, M. Ondrusek, H. Zhang, and D. K. Clark (2009), An oceanic cyclonic eddy on the lee side of Lanai Island, Hawai'i, *J. Geophys. Res.*, *114*, C10008, doi:10.1029/2009JC005346.

1. Introduction

[2] Lee sides of islands (headlands) are areas rich in eddy activities in terms of the direction of either winds or oceanic currents [e.g., Patzert, 1969; Signell and Geyer, 1991; Aristegui et al., 1994; Lumpkin, 1998; Barton et al., 2000; Barton, 2001; Chavanne et al., 2002; Dong and McWilliams, 2007; Calil et al., 2008]. There are two mechanisms for the eddy formation in the wake of islands: the one involves the oceanic response to wind stress curls and the other is oceanic island current wakes. For the former one, wind blocking due to the presence of islands can introduce positive (negative) wind stress curls on the right (left) side of the island while looking downstream, which causes upward (downward) Ekman pumping (see illustration by Chavanne et al. [2002] and Jimenez et al. [2008]). For the latter, as oceanic flow passes an island, the horizontal shear and inhomogeneity in bottom stress can induce vorticity. The mixture of two processes associated with the sheltering of wind from the island [Caldeira and Marchesiello, 2002] takes place with almost all islands, which makes the

scenario much more complicated. The Hawaiian Islands are located in the path of trade winds (quite steady northeasterly winds in this region) and the North Equatorial Current, so in principle, these two processes could be operative on the lee side of the island chain. In fact, eddies are ubiquitous on the lee side of the Hawaiian Islands [e.g., Patzert, 1969; Lumpkin, 1998; Chavanne et al., 2002; Dickey et al., 2008]. Cold core eddies are active agents promoting nutrient flux from depth to the euphotic zone, especially in the subtropic ocean, such as the area around the Hawaiian Islands, a so-called oceanic "desert" or oligotrophic ocean due to the existence of a subtropical gyre. These eddies are thus usually associated with high biological activity as reported in several papers within the past decade [e.g., Benitez-Nelson et al., 2007; Dickey et al., 2008; Rii et al., 2008; Nencioli et al., 2008; Kuwahara et al., 2008; Brown et al., 2008; Landry et al., 2008; Bidigare et al., 2003; Seki et al., 2001, 2002; Vaillancourt et al., 2003]. However the eddies' roles in the biological and biogeochemical processes remain enigmatic, partially because of the challenges of in situ eddy measurements due to the spontaneity in eddy generation and present technological limitations [Dickey and Bidigare, 2005]. Benitez-Nelson et al. [2007] and Benitez-Nelson and McGuillicuddy [2008] reported an extensive set of measurements of eddies on the lee side of the Big Hawaii Island in 2005. In particular, two eddies were extensively studied during their cruises on the lee side of the Big Island of Hawaii, an eddy-rich area [see Dickey et al., 2008].

[3] In this paper, we describe a cyclonic eddy observed around the mooring location of the Marine Optical Buoy

¹Institute of Geophysics and Planetary Physics, University of California, Los Angeles, California, USA.

²STAR, NESDIS, NOAA, Camp Springs, Maryland, USA.

³IMSG, Rockville, Maryland, USA.

⁴Department of Geography, University of California, Santa Barbara, California, USA.

⁵Raytheon Information Solution, Pasadena, California, USA.

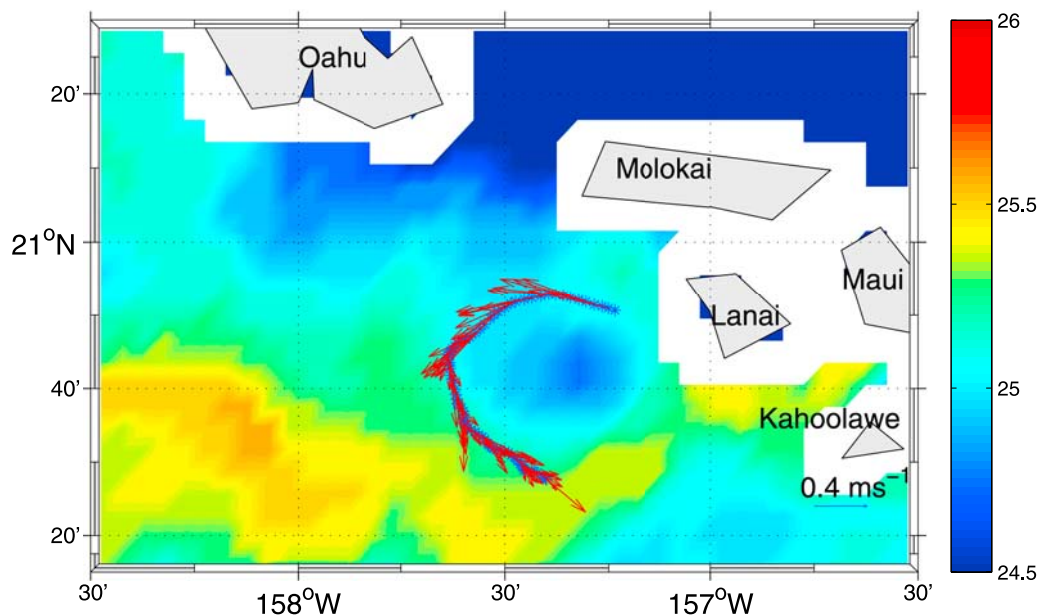


Figure 1. The trajectory of MOBY during the period after it broke free from its mooring and before it was recovered (18 December 1355 to 22 December 0303 UT). The blue stars are the GPS locations of MOBY and the red arrows depict the Lagrangian velocities estimated from the distance between two recording times. The color contours indicate the SST average for 19 and 20 December 2007 from GOES data with a resolution of about 5 km (units are in $^{\circ}\text{C}$).

(MOBY) offshore of Lanai Island, Hawai'i. The MOBY accidentally broke from its mooring and floated as a drifter for about 4 days in December 2007. The drifting locations of MOBY were recorded by its Argos, a satellite-based location system, and show that MOBY traveled in an anticlockwise (cyclonic) path offshore of Lanai Island. The tracking data and other satellite observations, such as the sea surface temperature (SST) and the chlorophyll concentration, are analyzed and all of them confirm that MOBY was following a cyclonic eddy on the lee side of Lanai Island. Altimetric sea surface height data are not used since the satellite tracks passed only over the edge of the eddy. A high-resolution numerical model is applied to the study and the numerical results show that eddies frequently occur on the lee side of Lanai Island. Finally, a statistical analysis of the numerical solution is reported.

[4] The paper is organized as follows: Section 2 demonstrates that MOBY followed a cyclonic eddy based upon the MOBY Argos location data and satellite data, the eddy's intensity is analyzed and its generation mechanism are discussed. Section 3 presents a numerical solution and its statistical eddy analysis based on an eddy detection scheme. The discussion and summary are presented in section 4.

2. Observations

2.1. A Cyclonic Eddy

[5] MOBY is the critical measurement platform for calibration of several ocean color sensing satellites including the Moderate Resolution Imaging Spectroradiometer (MODIS) and the Sea-viewing Wide Field-of-view Sensor (SeaWiFS). Approximately 15.24 m long, the spar buoy is the world's largest marine optical device. A physical oceanography group from the Moss Landing Marine Laboratories

constructed MOBY in 1991 and it (and a replacement twin MOBY) continues to be maintained at a site about 24 km offshore Lanai Island, Hawai'i. The site was chosen for its relatively clear sky conditions, low turbidity ocean waters, and moderate winds and waves (an island shadow zone with respect to prevailing northeast trade winds) [Clark *et al.*, 1997].

[6] Because of maintenance requirements, a MOBY platform has to be recovered and a replacement is redeployed at approximately 3-month intervals. A serial number is assigned for each individual deployment. The deployment number for the one of interest here from 10 September to 20 December 2007, is MOBY239; for more information about the MOBY, please refer to the website <http://physoce.mlml.calstate.edu/moby/> [also Clark *et al.*, 1997, 2003]. MOBY broke free from its mooring at 1352 UT 18 December and then drifted before it was recovered at 0303 UT 22 December. The period of the MOBY drifting time is 85.18 hours or 3.5 days. The number of the MOBY positions recorded by Argos is 116. The time intervals of position records are uneven, from 0.02 to 1.98 hours and the average time interval is 0.74 hours. The MOBY drifting trajectory is plotted in Figure 1, and shows that the free drifting MOBY traveled first northwestward, then turned southwestward on December 19, and continued its journey southeastward before it was recovered early December 22. MOBY made half an anticlockwise circle with a diameter of about 50 km during the drifting period. The rotating period for the eddy is comparable with that of cyclonic eddies observed on the lee side of Gran Canaria [Sangra *et al.*, 2007], which is 4.5 days.

[7] To determine if MOBY's trajectory followed that of a streamline for a cyclonic eddy, the daily sea surface temperature (SST) data from the Geostationary Operational Environmental Satellite (GOES) with the horizontal spatial resolution of 5 km are used. The 2-day averaged GOES SST

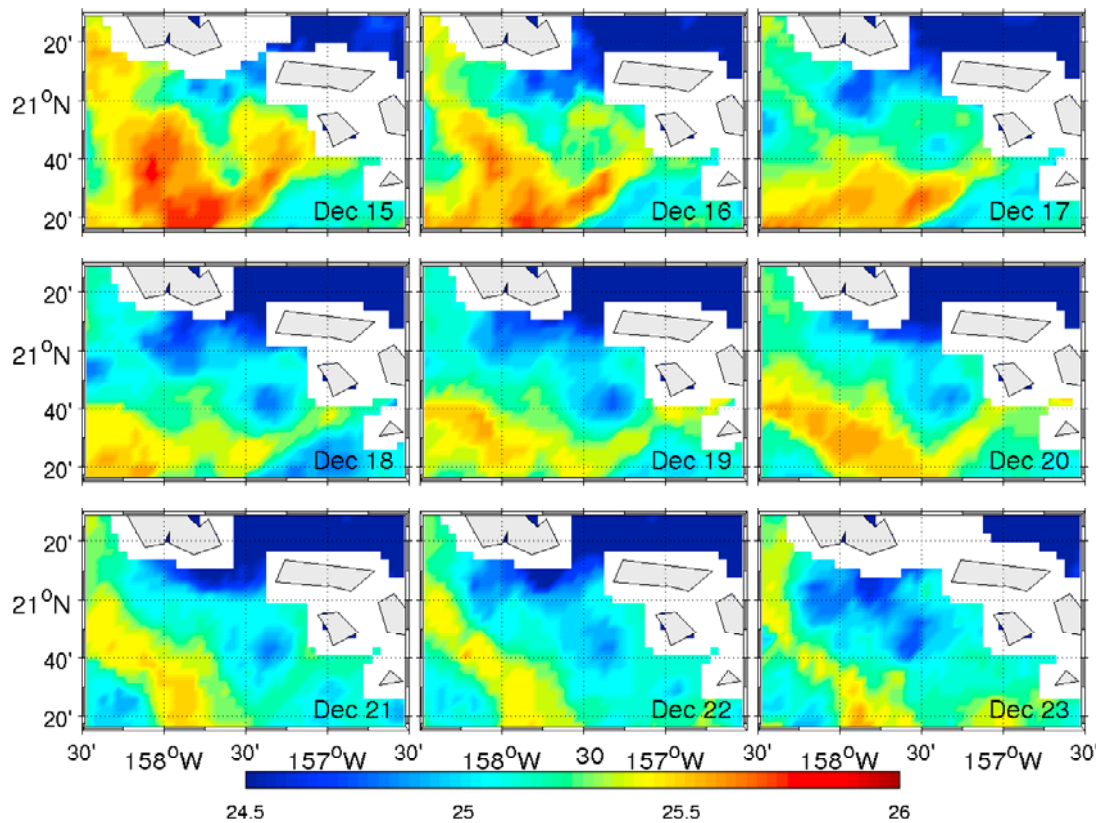


Figure 2. SST time series (units are in $^{\circ}\text{C}$) with 2-day average from the GOES data.

data are plotted Figure 1, and overlays the MOBY path. In the center of the incomplete anticlockwise circle of MOBY's trajectory lies cooler waters and the trajectory of the freed MOBY appears to generally follow the edge of the cold water, the expression of the cyclonic eddy. This suggests that the MOBY was indeed tracking a cyclonic eddy with a diameter of at least 50km. A cyclonic eddy likely upwells cold water from below to the surface in the vicinity of the eddy center (e.g., see realization by *Dickey et al.* [2008]). However, because of the thermocline depth and intensity of the eddy as well as possible surface overprints of warm waters, cool waters are not necessarily seen at the surface in the presence of a cyclonic eddy, thus, the age of a given cyclonic eddy is likely biased toward a lower estimate. Nonetheless, in this case, cooler surface waters are clearly evident.

[8] A time series of the mappings of SST in the area is shown in Figure 2 in order to further demonstrate that we have observed a cyclonic eddy and to investigate the lifetime history of the eddy. The 2-day averaged data are presented to reduce the impact of missing data (e.g., cloud obscuration issues). On 15–16 December, the area where MOBY would pass a few days later was still occupied by warm waters. On 16–17 December, a patch of slightly cooler water started to appear at the surface. On 17–18 December, distinctively cooler water could be seen in the area. On 18–19 December, when MOBY broke from its mooring, the circular cooler water patch was well developed and its evolution continued during 19–20 December. Its northwestern portion spread northward on 20–21 December, and split into pieces 1 day later. During 22–24 December, it started

to move northwestward and then merged with cooler water south of Oahu Island which was there since the beginning of the period. The development of the cyclonic eddy suggests that the cold water is formed locally, i.e., upwelled.

[9] Chlorophyll data collected during the period are examined to discern any response in the marine biological system (nutrient generated new primary productivity) associated with the eddy. Such data can provide additional observational evidence of the eddy. Again, the upwelling occurring from beneath the central portion of the cyclonic eddy would bring nutrients from below to the euphotic zone and the concentration of the chlorophyll could increase. Upwelling of the chlorophyll lying in the subsurface chlorophyll maximum could also come into play. The daily chlorophyll data observed from MODIS with spatial resolution of 9 km are used. The time series of the SST distributions in Figure 2 show that the eddy stayed near its original formation location for almost one week (17–22 December). This allows us to use multiple day averaged chlorophyll data to avoid the cloud contamination problem. The 8-day averaged MODIS satellite-based chlorophyll concentration data are shown in Figure 3. To compare with the SST spatial pattern, the SST distribution is also plotted in Figure 3 for the same period. The spatial pattern of the SST and the chlorophyll concentration match each other very well: the higher chlorophyll concentration and the lower SST are both south of Oahu Island and west of Lanai Island (in the cyclonic eddy area).

[10] In summary, both the SST and chlorophyll data suggest that eddy-related upwelling took place within an area described by an anticlockwise trajectory (radially

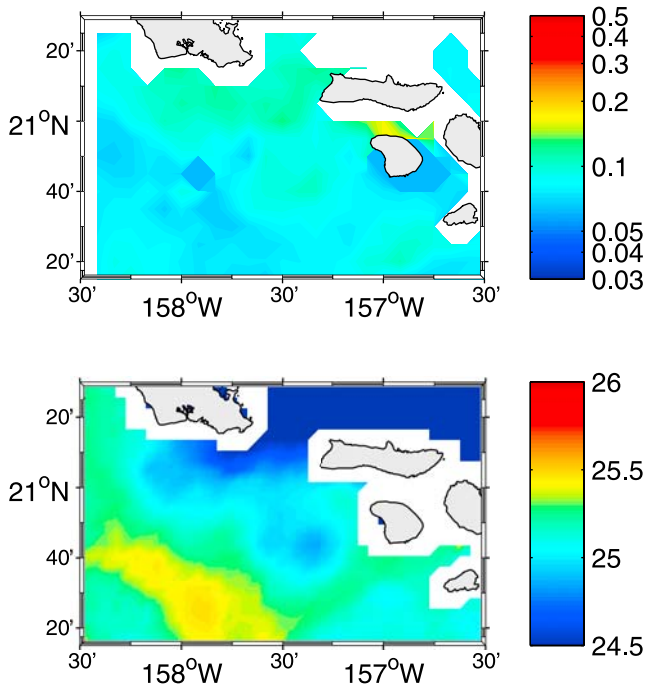


Figure 3. (top) The MODIS chlorophyll concentration (averaged over the period of 18–24 December 2007) at the sea surface during the period when the cyclonic eddy formed and developed. The colorbar is shown with a logarithmic scale and the data in the unit of mg m^{-3} . The data are based on the MODIS Aqua 9-km daily data. (bottom) The SST (also averaged over the period of 18–24 December 2007) from the GOES with the resolution of 5 km (units are in $^{\circ}\text{C}$). The spatial correlation between the chlorophyll concentration and SST is 0.76.

outward) of the freed MOBY made. This clearly demonstrates that the freed MOBY was following a mesoscale sized cyclonic eddy with a radius of at least 25 km.

2.2. Eddy Intensity

[11] To estimate the eddy intensity, the velocity of the eddy is calculated from the MOBY trajectory data. Figure 4a shows the drifting speed of MOBY. Before it turned eastward from westward, its speed was 46 cm s^{-1} . After its turning point, its speed decreased by a half and became 22 cm s^{-1} . When a drifter follows a streamline of a coherent eddy at a fixed radial distance from the eddy's center, its tangential speed should be constant (i.e., approximate solid body rotation at a given distance from the axis of rotation). To understand the dramatic change in the Lagrangian speed, the motion of MOBY is projected onto the zonal and meridional directions. From Figures 4a and 4d, it can be clearly seen how the change takes place. Along the zonal direction, the MOBY speed before and after it passed the west-east turning point decreased dramatically from 40.19 cm s^{-1} to 13.77 cm s^{-1} , however the speeds along the meridional direction do not change before and after the west-east turning point though there is small change at the turning point from the northward to southward. To understand this dramatic change in the speed, the velocity derived from the drift location data is decomposed into several terms according to its different momentum sources.

[12] MOBY was not designed to be a Lagrangian drifter, so points devoted to its forced motion bear discussion. After MOBY broke from the mooring, it oscillated at the air-sea interface. The wind, oceanic waves and eddy currents could all have varying degrees of direct effects on MOBY's motion. The Lagrangian current, derived from the Argos location data, can be decomposed as follows:

$$\begin{aligned} \mathbf{U}_{\text{lagran}} &= \mathbf{U}_{\text{euler}} + \mathbf{U}_{\text{stokes}} \\ &= \mathbf{U}_{\text{ekman}} + \mathbf{U}_{\text{geost}} + \mathbf{U}_{\text{res}} + \mathbf{U}_{\text{eddy}} + \mathbf{U}_{\text{stokes}}, \end{aligned} \quad (1)$$

where $\mathbf{U}_{\text{lagran}}$, $\mathbf{U}_{\text{euler}}$ and $\mathbf{U}_{\text{stokes}}$ are the Lagrangian, Eulerian and Stokes current, respectively. The Eulerian current $\mathbf{U}_{\text{euler}}$ includes four parts: the one is the Ekman drift $\mathbf{U}_{\text{ekman}}$ due to the sea surface wind, the sea surface geostrophic current $\mathbf{U}_{\text{geost}}$ due to the surface pressure, \mathbf{U}_{res} due to the nonlinearity, and \mathbf{U}_{eddy} is the azimuthal current around the eddy given the eddy shape is circular. The current for the eddy, i.e., the azimuthal velocity, is almost constant along the circular eddy at the presumed constant radial distance from the eddy's center.

[13] The first three terms on the right side of equation (1) are the large-scale current, i.e., the background flow. The nonlinear residual is generally small for the large-scale current [Dong *et al.*, 2009]. The Ekman drifting current $\mathbf{U}_{\text{ekman}}$ is theoretically directed 45° toward the right facing toward the wind direction in the northern hemisphere, however in real geostrophic flows, the deflection angle is much less than 45° and is found to range between 5° and 20° [Cushman-Roisin, 1994]. The daily blended wind data with the QuikSCAT satellite-based wind product [Zhang *et al.*, 2006] show the wind direction is almost uniform northeasterly (Figure 5) and constant from 10 December to the end of December at about 75° on the basis of the meteorological wind direction convention (Figure 6). The MOBY Ekman drift is generally in the westward direction with slightly northward by 5° on the basis of the above estimate of the deflection angle. The surface Ekman drifting current is $\mathbf{U}_{\text{ekman}} = \frac{2\mathbf{k} \times \boldsymbol{\tau}}{\rho f D}$, where \mathbf{k} is the vertical unit vector, $\boldsymbol{\tau}$ wind stress, f the local Coriolis coefficient, ρ the water density, D is the Ekman layer thickness, which is estimated by $D = \frac{0.4}{f} \sqrt{\frac{\tau}{\rho}}$ as 76 m [Cushman-Roisin, 1994]. The coefficient 2 is due to the assumption that the linear change in the velocity in the Ekman layer. Given the wind stress is about 0.1 N/m^2 from Figure 6, $\mathbf{U}_{\text{ekman}} = 5.0 \text{ cm/s}$. The altimeter-measured sea surface height data from the Archiving, Validation, and Interpretation of Satellite Oceanographic data (AVISO) product (<http://www.aviso.oceanobs.com>) are used to estimate the geostrophic current, and it is about 5.0 cm/s westward.

[14] The wave-induced mass transport, i.e., Stokes drift velocity can be estimated theoretically, \mathbf{u}^{St} , as [e.g., LeBlond and Mysak, 1978]

$$\mathbf{u}^{\text{St}} = \frac{H_{\text{sig}}^2 \omega \mathbf{k} \cosh 2k(z+h)}{8 \sinh^2 kh} \quad (2)$$

along with the linear dispersion relation

$$\omega^2 = gk \tanh kh, \quad (3)$$

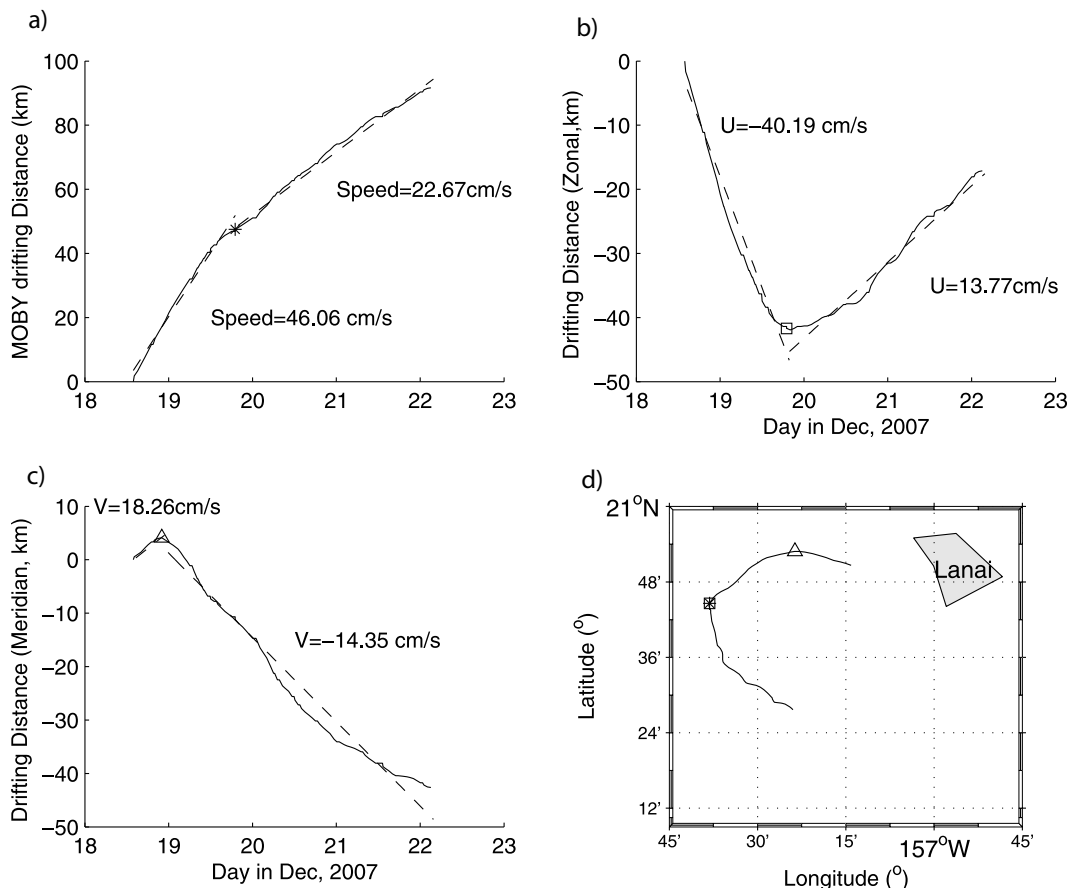


Figure 4. (a) The solid line is the drifting distance of MOBY from the breaking point versus the time, and the dashed lines are the linear regressions for two periods separated by the star at the turning point where MOBY drifted from westward to the eastward. (b) The solid line is the drifting distance projected on the zonal direction versus the time, and the dashed lines are the linear regressions for the two periods separated by the square at the turning point. (c) The same as Figure 4b except for the distance projected on the meridional direction and the separated point is marked by the triangle at the turning point from northward to southward. (d) The trajectory of MOBY. The numbers are the slope of the linear regression lines, which is the velocity or speed of MOBY for specified period.

where H_{sig} is significant wave height; z is vertical coordinate ($z = 0$ for the surface drift); h is local water depth; ω is wave frequency; \mathbf{k} is wavenumber vector and k is its magnitude; and g is the gravitational constant. We make use of the in situ wave data from two National Data Buoy Center (NDBC) roll-pitch buoys (<http://www.ndbc.noaa.gov/>) northwest of Kauai Island, HI (NDBC 51001, 23.445°N & 162.279°W) and at Christmas Island (NDBC 51028, 0.0°N & 153.913°W), both of which measured H_{sig} , ω and \mathbf{k}/k required for the \mathbf{u}^{St} estimation. From 18 December to 20 December, the meridional component of 2 cm/s equatorward is much smaller compared with the zonal component, which is about 5 cm/s westward. Since 20 December, the southwesterly waves were predominant, both the meridional and zonal components of \mathbf{u}^{St} are in the same magnitude of about 2 cm/s (Figure 7). To get wave data near the eddy site, a global NOAA-National Center for Environmental Prediction (NCEP) wave hindcast product with the Wave Watch III (WW3) model [Tolman, 2002] at (157.5°W , 21.0°N), near the eddy area, is used. The data and model production descriptions are available at <http://polar.ncep.noaa.gov/waves/index2.shtml>. The model grid

spacing is 1.0 degree in the meridional direction and 1.25 degree in the zonal direction, and the data output is sampled every 3 hours. The Stokes drift derived the wave model data is in the same scale of the magnitude as those from NDBC Buoy, see Figure 7.

[15] In summary, the dramatic change in the Lagrangian current in the zonal direction before and after the west-east turning point is due to the Ekman drift and geostrophic current (the residual current can be neglected). The small change in the Lagrangian current in the meridional direction in the course of the MOBY drifting is because the Ekman drift and the geostrophic current are neglectable and the Stokes drift is in a small magnitude. In the first order of approximation, before the east-west turning point (see Figure 4), the mean zonal speed for the eddy can be estimated as $\mathbf{U}_{eddy} = \mathbf{U}_{lagran} - \mathbf{U}_{ekman} - \mathbf{U}_{geost} - \mathbf{U}_{stokes} = -40.19 + 5.0 + 5.0 + 5.0 = -25.19$ cm/s. For the mean meridional speed for the eddy is $\mathbf{V}_{eddy} = \mathbf{V}_{lagran} - \mathbf{V}_{ekman} - \mathbf{V}_{geost} - \mathbf{V}_{stokes} = -14.35 + 2.0 = -12.35$ cm/s, where \mathbf{V}_{ekman} and \mathbf{V}_{geost} are neglectable. After the east-west turning point, the Lagrangian current \mathbf{U}_{lagran} decreases to 13.77 cm/s and on the basis of the similar calculation as above, the

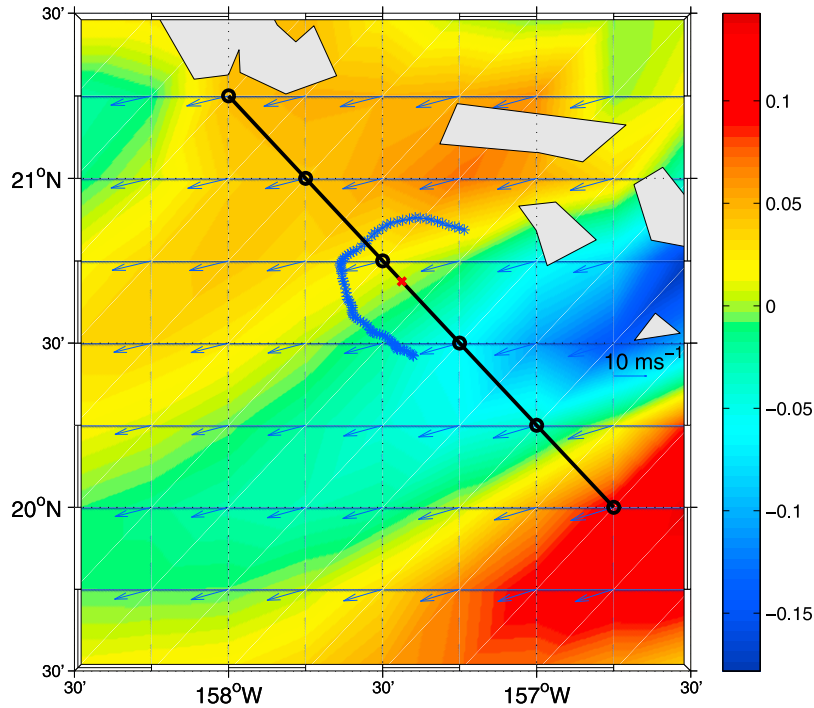


Figure 5. Daily averaged merged wind [Zhang *et al.*, 2006] on 15 December (the onset of the cyclonic eddy). The blue vectors are the wind vectors (units are in m/s) and the wind stress curls are plotted in color contours (units are in Pa/100 km). Blue stars are the MOBY locations, and the black solid line is the transection across the center of the eddy during the MOBY drifting period. The black circles on the solid line denote wind data points (see Figure 8). The red cross indicates the center of the eddy. The wind direction is about 75.0° (the direction the wind is coming from is in degrees clockwise from true north according to the meteorological convention). The wind direction persists in this direction from 10 to 26 December with a standard deviation of about 5.0° .

eastward $U_{\text{eddy}} = 28.77 \text{ cm/s}$, which is very close to the westward Eulerian current before the turning point, reflecting the circular eddy shape. On the basis of the above estimate, the azimuthal current for the eddy is about 30.0 cm s^{-1}

in magnitude (averaged from westward and eastward currents).

[16] The current for the eddy could be caused by either the flow instability or wind stress curl. Given that the

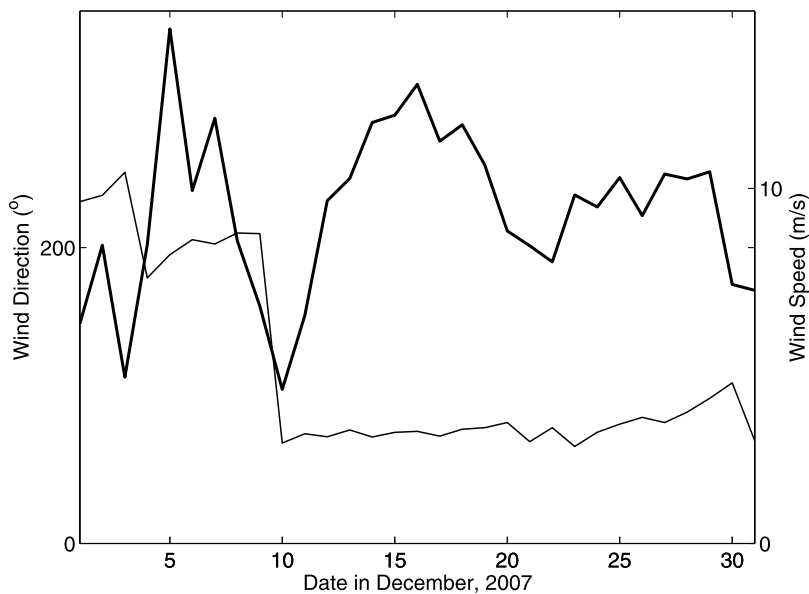


Figure 6. Time series of the daily wind direction (thin line) and speed (thick line) at the point which is the closest wind data point to the center of the eddy. The direction the wind is coming from is in degrees clockwise from true north according to the meteorological convention.

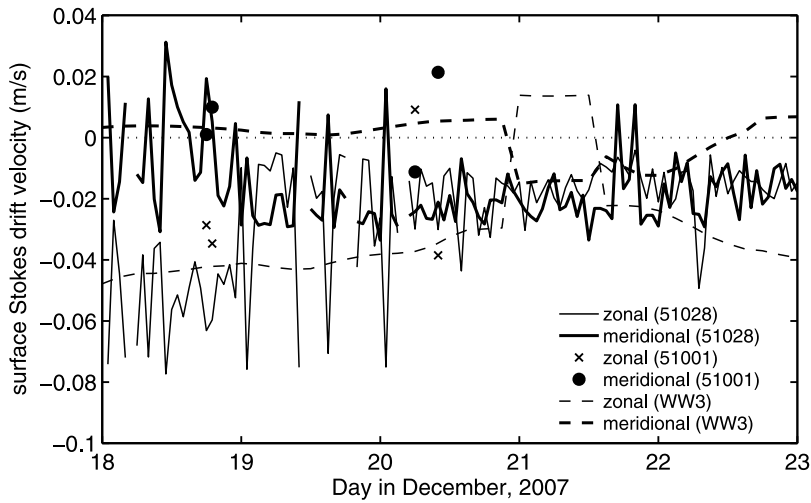


Figure 7. Stokes drifter velocities inferred from the NDBC buoys and a NCEP global wave model (WW3). The following two buoys which are the closest NDBC buoys carrying the wave data are used: 51028 (0.0°N, 153.913°W) and 51001 (23.445°N, 162.279°W). The wave model data are located at 21.0°N, 157.5°W.

radius of the trajectory from the center of the eddy is about 25 km, the vorticity of the eddy is about $1.2 \times 10^{-5} \text{ s}^{-1}$, which is comparable with the background rotating rate $2.5 \times 10^{-5} \text{ s}^{-1}$. The divergence scale of the eddy is also $1.2 \times 10^{-5} \text{ s}^{-1}$, and thus the upward vertical velocity is

about $0.9 \times 10^{-3} \text{ m/s}$ (77.8 m/d) if the mixing layer is in the same scale of the Ekman layer.

2.3. Discussion on Eddy Generation

[17] The time series of the SST from the GOES (Figure 2) show the cooler temperature at the eddy site is generated

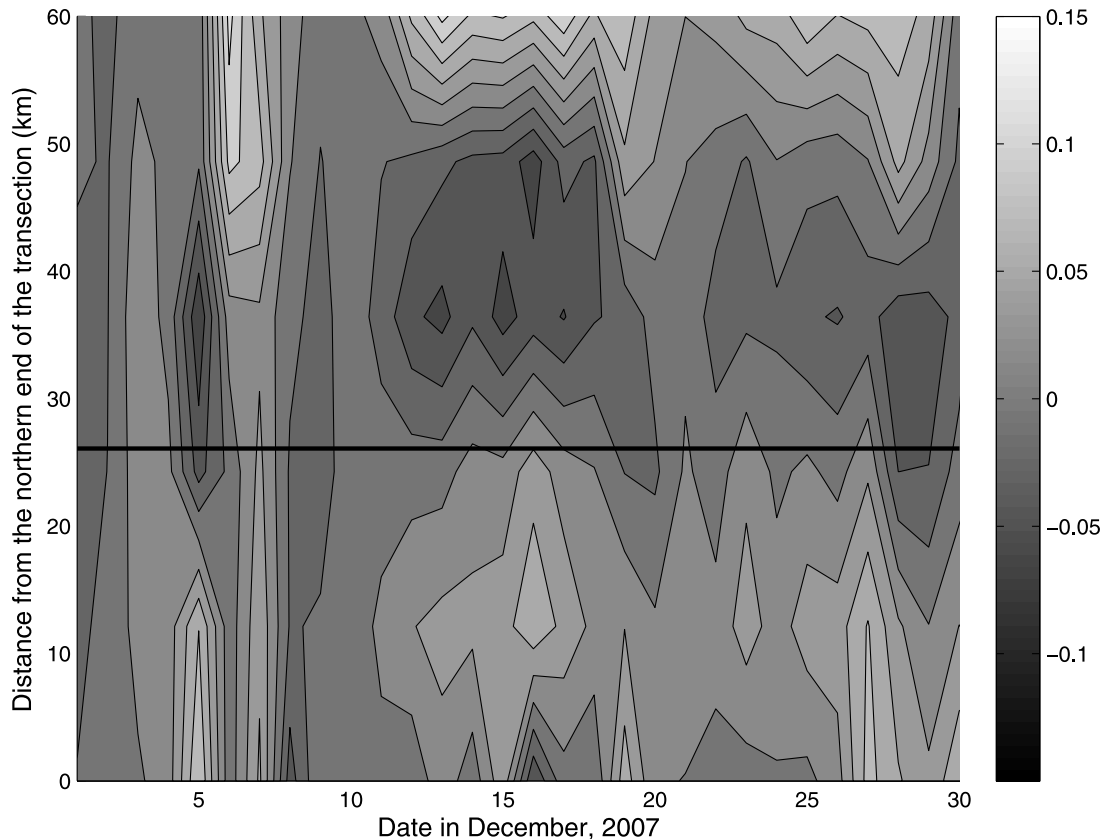


Figure 8. Time series of the daily wind stress curl along the transection (see Figure 5). The units are in Pa/100 km. The black line denotes the location of the eddy center during the MOBY drifting period.

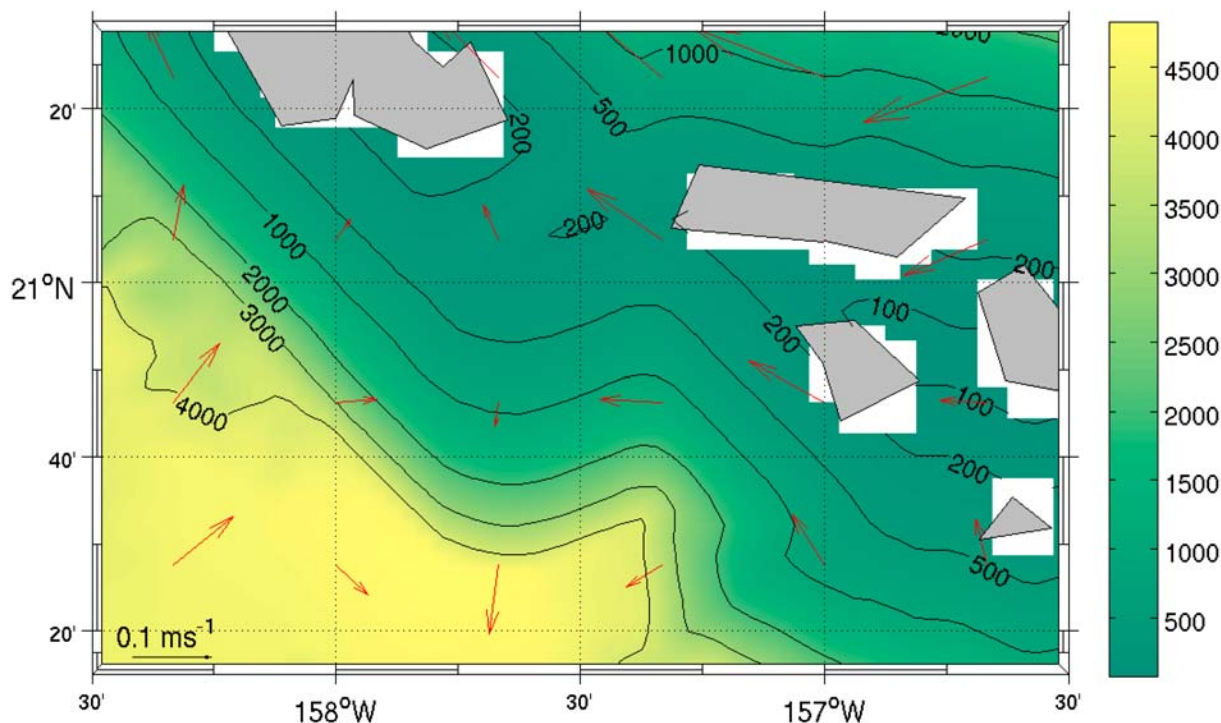


Figure 9. The geostrophic current averaged for 19–20 December 2007 (arrows) and the bathymetry (contours). The former is from the daily AVISO product with the spatial resolution of $1/3^\circ \times 1/3^\circ$, merged from multiple satellite altimetry data. The latter is from ETOPO2 bathymetry data (units are in m). The coastline data are from the M-MAP (a set of mapping tools written for Matlab version 5 and later) package, shown in the gray blocks. The black blocks are islands resolved by the ETOPO2 data.

locally other than remotely. It implies the eddy could be generated by the local external forcing such as wind stress curl or a local flow instability. Because of the lack of local measurements of the oceanic current or the vertical profile of the density and current, we have no clue if any flow instability took place at the time when the eddy was formed. However the time series of the wind speed (Figure 6) show a sudden increase in the wind speed on 15 December, the date of the onset of the cyclonic eddy, which results in a significant increase of the wind stress curl on the northside of the center of the eddy on 15 December, see Figure 8. The burst of a high wind is coincident with the appearance of the cooler water timely, which suggests the eddy could be induced by the local wind stress curl [Pullen *et al.*, 2008].

[18] Interaction of the oceanic flow with the bottom topography is also a possible mechanism to generate the cyclonic eddy. Figure 9 shows the bottom topography (contours) and the surface geostrophic currents averaged over 19 and 20 December 2007. The surface geostrophic current data are downloaded from the AVISO product: <http://www.aviso.oceanobs.com/en/home/index.html>. The AVISO geostrophic currents are calculated from multiple satellites altimetry sea surface height data with the resolution of $1/3^\circ \times 1/3^\circ$ and daily sampled. The surface oceanic current flows along the island chain northwestward. On the lee side of islands, the large-scale circulation is an anticyclonic gyre. The sharp change (a trench) in the water depth west of the Lanai Island could induce cyclonic eddies, however, because of the resolution limit, the AVISO data cannot resolve the eddy tracked by the MOBY. A high-

resolution model simulation could provide a solution, see section 3.

3. Numerical Simulation

[19] To further examine the eddy activity and dynamics on lee side of Lanai Island, the Regional Oceanic Modeling System (ROMS) is utilized. ROMS solves the rotating primitive equations. It is a split explicit, free surface oceanic model, where short time steps are used to advance the surface elevation and barotropic momentum equations, with a larger time step used for temperature, salinity, and baroclinic momentum [Shechepetkin and McWilliams, 2005]. A third-order, upstream-biased advection operator allows the generation of steep gradients in the solution, enhancing the effective resolution of the solution for a given grid size when the explicit viscosity is small. The numerical diffusion implicit in the upstream-biased operator allows the explicit viscosity to be set to zero without excessive computational noise or instability. (For detailed discussion on zero explicit viscosity, please refer to Dong *et al.* [2007].) It has been demonstrated that the ROMS can reproduce mesoscale eddies observed on the lee side of the Big Island of Hawai'i [Calil *et al.*, 2008].

[20] We developed two-level offline nesting grids using the Regional Oceanic Model System (ROMS) (L_1 is $1/10$ degree and L_2 is $1/32$ degree). The model is forced by the 2007 daily blended wind data with the 25 km resolution [Zhang *et al.*, 2006]. The open boundary data are from the monthly SODA data set [Carton *et al.*, 2000a, 2000b]. The

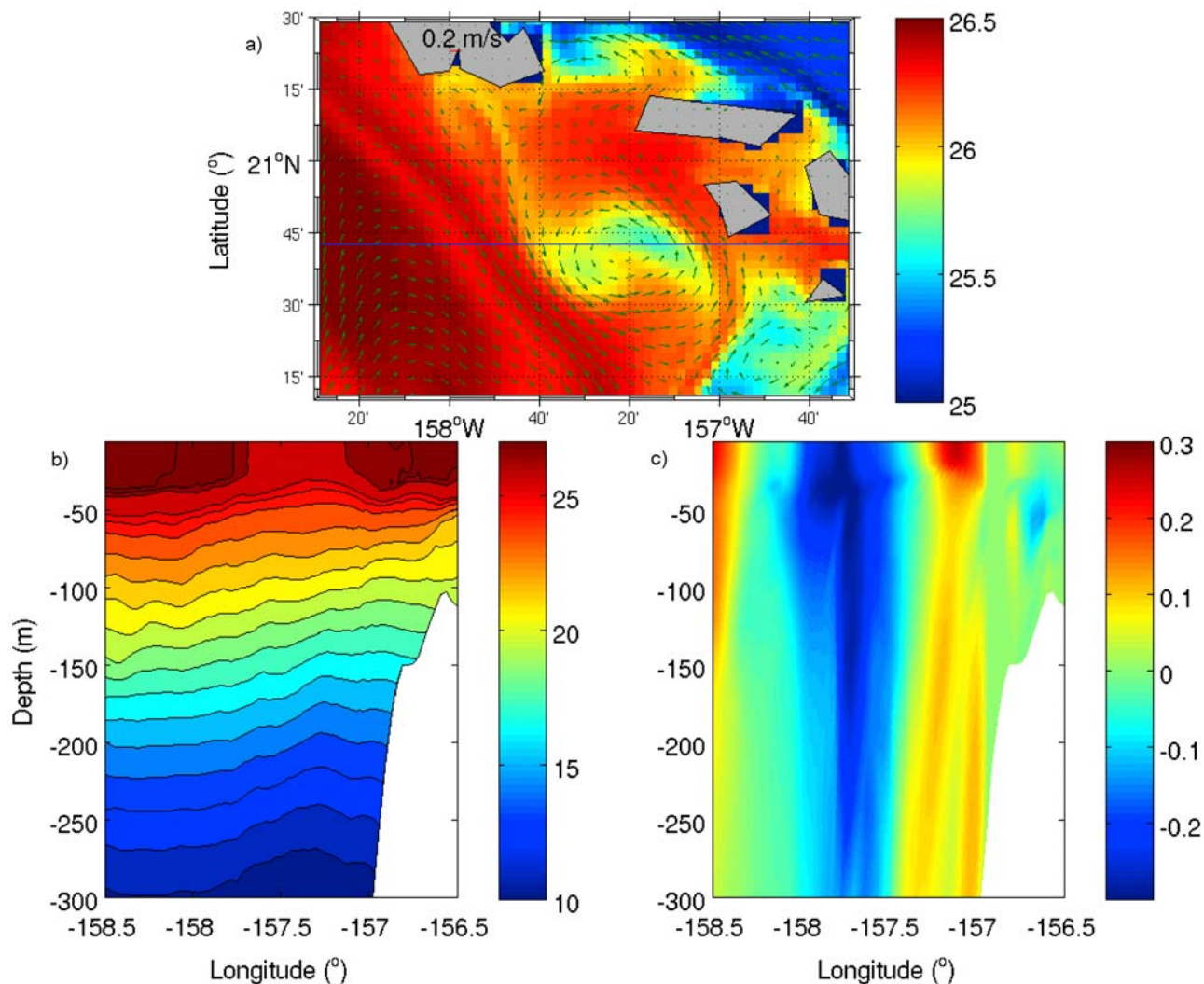


Figure 10. A typical example of cyclonic eddies evident offshore Lanai Island using results from the ROMS numerical simulation. During the 3-year repeated runs, the cyclonic eddies could appear at different times at the different years. (a) The surface current and temperature (units are in °C), and (b) the vertical profiles of the temperature (units are in °C) and (c) the meridional velocity (units are in m/s).

model is repeated for four years. The last three years are analyzed. The mean circulation of the last three years is compared with the drifter-derived climatological surface current and shows its consistency with the circulation derived from the drifter data (Lumpkin and Garraffo [2005] data are available online at <http://www.aoml.noaa.gov/phod/dac/drifter-climatology.html> and an analysis by Qiu *et al.* [1997]). West of the Hawaiian Islands and downstream of generally prevailing northeasterly trade wind, North Equator Current (NEC), cyclonic and anticyclonic eddies are frequently generated and propagate generally northwestward and southeastward, respectively [Calil *et al.*, 2008]. In Figure 10, a cyclonic eddy with a similar location to that described by our observations and with comparable intensity is selected for comparison and analysis. The similarity allows us to examine the vertical structure and variability of a model-generated cyclonic eddy which is not possible due to data unavailability for the observed eddy. The signature of the eddy can be seen as deep as 300m. This depth of impression is comparable to

those of Cyclones Noah and Opal off Hawaii observed during the E-Flux field experiment and reported by Dickey *et al.* [2008], Kuwahara *et al.* [2008], and Nencioli *et al.* [2008].

[21] Statistical analysis of the eddies in the area of the MOBY drift pattern is performed. In particular, we developed an eddy detection algorithm to do statistical analysis of the eddies that were generated and passed through the study area. The algorithm directly uses oceanic currents to detect vorticity on the basis of the minimum speed and the reversal in velocity direction (see Appendix A and also F. Nencioli *et al.* (A vector geometry based eddy detection algorithm and its application to high-resolution numerical model products and high-frequency radar surface velocities in the Southern California Bight, submitted to *Journal of Atmospheric and Oceanic Technology*, 2009) for the details), which is an algorithm different from other existing approaches: Okubo-Weiss Parameter [Isern-Fontanet *et al.*, 2003; Chelton *et al.*, 2007], the wavelet analysis [Siegel and Weiss, 1997; Doglioli *et al.*, 2007] and the winding

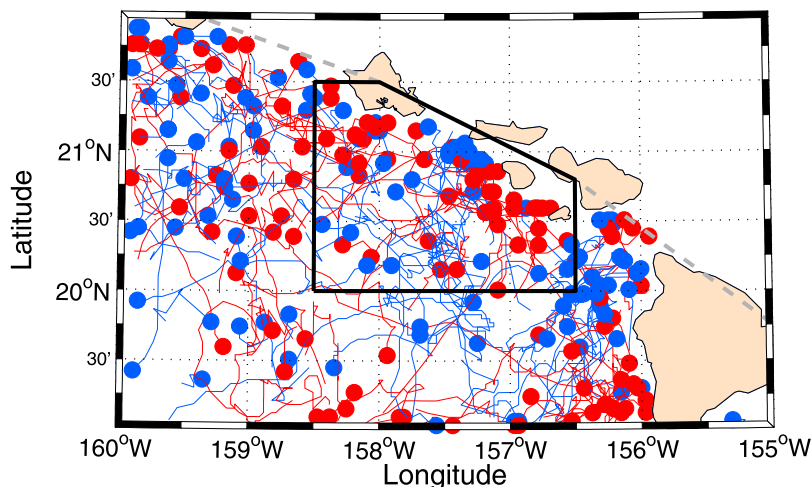


Figure 11. Trajectories of modeled eddies on lee side of the Hawaii Islands in the repeated 3 years of ROMS simulation. The modeled current data are sampled daily. Circles denote the eddy generation sites. Red circles indicate anticyclonic eddies and blue circles show cyclonic eddies. The thin lines are the trajectories of eddies (again red for anticyclonic and blue for cyclonic). The patterns shows that on the northern (southern) lee flank of Hawai'i Island there are more cyclonic (anticyclonic) eddies generated. The box is the area where the statistic analysis is applied. On the northern (southern) lee flank of the group of middle islands, there are more cyclonic (anticyclonic) eddies. This is consistent with the argument that there is symmetry in cyclonic and anticyclonic eddy generation on the lee side of an island.

angle method [Sadarjoen and Post, 2000; Chaigneau *et al.*, 2008]. Figure 11 shows the trajectories of eddies generated over the course of three years. An interesting pattern is evident: i.e., on the northern (southern) lee flank of the group of islands in the chain including the Big Island of Hawaii, generally more cyclonic (anticyclonic) eddies are evident in the model results. This is consistent with the argument that there is north-south symmetry in cyclonic and anticyclonic eddy generation on the lee side of an island. When the trade winds (northeasterly generally) pass the islands from the east, the positive (negative) wind stress curl is generated on the north (south) flank of the lee side of the islands, which could induce the cyclonic (anticyclonic) eddies [Dong *et al.*, 2007; Chavanne *et al.*, 2002]. When the westward NEC approaches the islands, the current shear instability could enhance such eddy generation [Calil *et al.*, 2008].

[22] We next focus specifically on the lee side of Lanai Island (158.5°W–156.5°W, 20°N–21.5°N, see Figure 10). The statistical results of the eddies in the area are listed in Table 1. The daily eddy number and eddy sizes detected in the area are similar for cyclonic and anticyclonic eddies. The average lifetime for a cyclonic eddy is somewhat longer than for an anticyclonic eddy. The lifetime of an eddy is only for the time when the eddy is within the numerical domain therefore the lifetime is underestimate of the actual lifetime. This is in agreement with work reported by Jin *et al.* [2009]. The intensities of cyclonic eddies are also relatively greater than for the anticyclonic eddies in terms of relative vorticity, SST and SSH anomalies.

4. Summary and Discussion

[23] The optical buoy MOBY is a primary in situ observation platform used to calibrate the MODIS and SeaWiFS.

MOBY broke free from its mooring off Lanai Island on December 18, 2007 and was recovered on Dec 22, 2007. During MOBY's about 4-day drift at sea, it tracked a cyclonic eddy on the lee side of Lanai. The cyclonic eddy was evident in the satellite remote sensing data: chlorophyll from MODIS, SST from GOES. The time series of satellite-based SST show that the cold core eddy was likely young in age: for about 9 days it was clearly a distinctive eddy but then it merged with cold waters south of Oahu Island. An increase in chlorophyll concentration within the young cold core eddy suggests nutrient export from depth to the surface (upwelling at the eddy center), which is vital to the marine primary productivity in the oligotrophic ocean (nutrient-deficient water). The dramatic changes in the Lagrangian velocity of MOBY are due to the westward Ekman drift and background geostrophic current. The estimate of its intensity shows it is a strong eddy.

Table 1. Cyclonic and Anticyclonic Eddy Statistics Averaged Over 3 Years of Simulation^a

| Property | Cyclonic | Anticyclonic |
|------------------|----------------|---------------|
| population | 0.69 ± 0.74 | 0.73 ± 0.74 |
| radius (km) | 16.43 ± 13.11 | 13.26 ± 11.44 |
| lifetime (days) | 17.17 ± 29.35 | 13.14 ± 13.22 |
| δSST (°C/100 km) | 1.15 ± 0.82 | 0.64 ± 0.53 |
| η'/f_0 | 0.96 ± 0.38 | -0.91 ± 0.36 |
| SST' (°C) | -0.40 ± 0.38 | 0.10 ± 0.29 |
| SSH' (m) | -0.075 ± 0.072 | 0.053 ± 0.049 |

^aAll eddies with a lifetime longer than 4 days were included in the computation. Population is the average number of cyclones and anticyclones inside the area at any given day. The δSST is the average value of the mean amplitude of the temperature gradient within each eddy. Here η'/f_0 , SST', and SSH' are the averages of the maximum anomalies found within the eddies. The anomalies were computed with respect to the spatial mean of the day the eddy was detected. The standard deviations are presented after the ± signs.

[24] An offline two-level nesting numerical model (ROMS) was applied to simulate the eddy formation and evolution on the lee side of Lanai Island. The high-resolution numerical simulation shows the frequent existence of mesoscale eddy activities on the lee side of Lanai. To detect the eddies in the area, an eddy detection algorithm based on the velocity field was developed. The statistical result shows that the populations and sizes of cyclonic and anticyclonic eddies are similar, but the lifetimes of cyclonic eddies are longer than those of anticyclonic eddies and the intensities of cyclonic eddies are greater than those of anticyclonic eddies.

[25] The present analysis of the trajectory of the free-drifting MOBY is incorporated with the satellite observational data. During the lifetime of the observed eddy, there were no other in situ data available. Looking forward, it may be possible in the future to utilize surface drifter data by applying automated trajectory-tracked eddy detection schemes to detect eddies [e.g., *Lankhorst, 2006; Boebel et al., 2003; Lilly and Gascard, 2006*], and then assemble satellite data within eddy areas to quantify eddy features and their physical and biogeochemical impacts in the world ocean given that more and more drifters and satellite data are becoming available [*Lumpkin and Pazos, 2007*].

Appendix A: Eddy Detection and Tracking Algorithm

[26] This appendix briefly describes the algorithm developed for this study to objectively detect and track mesoscale eddies. A more exhaustive and complete description of the method, which was inspired by E-Flux ship-based operations, will be presented in a separate paper by Nencioli et al. (submitted manuscript, 2009).

[27] Mesoscale eddies can be defined as structures of the flow field where the velocity vectors rotate around a center. The velocity fields associated with mesoscale cyclones and anticyclones are characterized by common features, such as a velocity minimum in proximity of their centers, and tangential velocities that increase approximately linearly with distance from the center before reaching a maximum value and then decreasing. Furthermore, because of the rotational nature of the motion, the meridional or v component of velocity reverses in sign along an east-west section across an eddy center, and the westward or u component reverses in sign along a north-south section. A recent study of a mesoscale cyclone (Cyclone Opal) sampled in the lee of the Big Island of Hawaii showed that these features can be successfully used to estimate the location of an eddy's center [*Nencioli et al., 2008*]. The detection algorithm used in this study was developed using the same concept. Eddy detection is based entirely on the geometry of the surface velocity fields.

[28] Existing eddy detection algorithms are either based on the distribution of physical quantities such as the Okubo-Weiss parameter [i.e., *Isern-Fontanet et al., 2003; Chelton et al., 2007*], or the vertical component of relative vorticity [*Doglioli et al., 2007*]; or they are hybrid methods in which a physical quantity (i.e., Sea Level Anomaly) is used to detect eddy centers, and then the geometrical characteristics of the flow field (i.e., instantaneous streamlines) are used to derive eddy dimensions [*Chaigneau et al., 2008*]. We

developed a new method as an alternative to the existing ones, because preliminary results using the Okubo-Weiss parameter (not shown) revealed that features such as strong frontal regions as well as the shear regions in the island wakes are often wrongly detected as mesoscale eddies since they are characterized by similar values; furthermore, a purely geometrical method would allow to detect also those eddies that are not characterized by a strong SLA minima or maxima.

[29] Four constraints were derived in conformance with the general characteristics associated with the eddy's velocity field and eddy centers at hose grid points where all the constraints are satisfied. The four constraints follow:

[30] 1. The v component of velocity has to reverse in sign along a east-west section across the eddy center, and its magnitude has to increase a points away in both eastward and westward directions away from it.

[31] 2. The u component of velocity has to reverse in sign along a north-south section across the eddy center, and its magnitude has to increase a points away in both southward and northward directions away from it. The sense of rotation has to be the same as for the v component.

[32] 3. The eddy center is characterized by the minimum in velocity magnitude within the region that extends up to b grid points around it.

[33] 4. The direction of the velocity vectors at $a - 1$ grid points around the eddy center have to change with a constant sense of rotation, and the directions of two neighboring velocity vectors have to lay within the same, or two adjacent quadrants (the four quadrants are defined by the north-south and west-east axes; the first quadrant encompasses all the directions from east to north, the second quadrant the directions from north to west, the third quadrant the directions from west to south, and the fourth quadrant the directions from south to east).

[34] The two parameters a and b had to be defined in order to optimize the automated eddy detection. Following *Chaigneau et al. [2008]*, the algorithm results for different combination of a and b were compared to the results from manual detection for 10 days randomly selected among the 1080 available. The best performance was obtained for $a = 3$ and $c = 2$: among the 85 eddies which were manually detected, 76 were successfully detected by the algorithm (success of detection $\approx 89.4\%$), and only 3 points were wrongly detected as eddy center (excess of detection $\approx 3.5\%$).

[35] Once the eddy centers are detected, the size of each eddy are determined using streamfunctions. Since velocity fields associated with mesoscale eddies are characterized by weak divergence, contour of the stream function are, to a first order, streamlines. Eddy limits are defined as the largest closed streamline around the eddy center. As a further constraint, the velocity magnitude has to increase radially across the closed streamline. This condition is included in order to physically define the eddy boundary as the point at which tangential velocity begins to decrease. The radius of each eddy is then computed as the mean distance between the center of the eddy and the eddy limits using this formalisms. The adopted definition of eddy boundary results in a conservative estimate of eddy sizes. However the method is consistent, since visually larger eddies are characterized by larger boundaries.

[36] An eddy is tracked by comparing the position of its center at successive time steps (daily output in this case). The track of a given eddy is updated from time step t to time step $t+1$ by looking for eddy centers of the same type (cyclonic or anticyclonic) within a searching area of 15 numerical grid points (approximately 48 km) at $t+1$, centered at the location of the eddy at t . If a center cannot be located, then the search is performed at $t+2$, and the searching area increased to 21 grid points (approximately 68 km) (this is to prevent the algorithm from recording two distinct eddies, the same eddy was not be detected during a particular day because it is too weak or too asymmetric). If even at $t+2$ no centers are detected, then the eddy is considered dissipated and the track for that specific eddy is closed. Again, the eddy tracking illustrated in Figure 11 followed this methodology. Lifetime of each eddy is computed as the difference between the last and the first day on record for each track. Since a track is interrupted if the eddy abandon the domain, the values obtained are in several cases underestimates of real eddy lifetimes.

[37] **Acknowledgments.** C.D. and J.C.M. appreciate supports from the National Science Foundation (OCE 06-23011) and the National Aeronautics and Space Administration (grant NNX08AI84G). T.M. appreciates the support of the GOES-R program office. F.N. and T.D. acknowledges support from the National Science Foundation (grants OCE 0241121 and OCE 0754095) and his Secretary of the Navy/Chief of Naval Operations Chair in Oceanographic Sciences (grant N00014-08-1-1178). The MOBY is operated by the team from the Moss Landing Marine Laboratory, California State University. The team includes M. Yarbrough, M. Feinholz, T. Houlihan, D. Peters, S. Flora, Y. Kim, E. Stengel, and M. Murphy. Comments from two anonymous reviewers helped improve the manuscript. The contents of this paper are solely the opinions of the authors and do not constitute a statement of policy, decision, or position on behalf of NOAA or the U.S. Government.

References

- Aristegui, J., P. Sangra, S. Hernandez-Leon, M. Canton, A. Hernandez-Guerra, and J. Kerling (1994), Island-induced eddies in the Canary Islands, *Deep Sea Res. Part I*, *41*, 1509–1525.
- Barton, E. (2001), Island wakes, in *Encyclopedia of Ocean Sciences*, vol. 5, edited by J. H. Steele, S. A. Thorpe, and K. K. Turekian, pp. 1397–1402, Academic, Orlando, Fla.
- Barton, E., G. Basterretxea, P. Flament, E. Mitchelson-Jacob, B. Jones, J. Aristegui, and F. Herrera (2000), Lee region of Gran Canaria, *J. Geophys. Res.*, *105*, 17,173–17,193.
- Benitez-Nelson, C., and D. J. McGillicuddy Jr. (Eds.) (2008), Mesoscale Physical-Biological-Biogeochemical Linkages in the Open Ocean: Results from the E-FLUX and EDDIES Programs, *Deep Sea Res.*, *55*(10–13), 1133–1518.
- Benitez-Nelson, C. R., et al. (2007), Mesoscale eddies drive increased silica export in the subtropical Pacific ocean, *Science*, *316*, 1017–1021, doi:10.1126/science.1126221.
- Bidigare, R. R., C. Benitez-Nelson, C. L. Leonard, P. D. Quay, M. L. Parsons, D. G. Foley, and M. P. Seki (2003), Influence of a cyclonic eddy on microheterotroph biomass and carbon export in the lee of Hawaii, *Geophys. Res. Lett.*, *30*(6), 1318, doi:10.1029/2002GL016393.
- Boebel, O., J. Lutjeharms, C. Schmid, W. Zenk, T. Rossby, and C. Barron (2003), The Cape Cauldron: A regime of turbulent inter-ocean exchange, *Deep Sea Res. Part B*, *50*, 57–86.
- Brown, S. L., M. R. Landry, K. E. Selph, E. J. Yang, Y. M. Rii, and R. R. Bidigare (2008), Diatoms in the desert: Plankton community response to a subtropical mesoscale eddy in the North Pacific, *Deep Sea Res. Part II*, *55*, 1321–1333.
- Caldeira, R. M. A., and P. Marchesiello (2002), Ocean response to wind sheltering in the Southern California Bight, *Geophys. Res. Lett.*, *29*(13), 1635, doi:10.1029/2001GL014563.
- Calil, P. H. P., K. Richards, Y. Jia, and R. Bidigare (2008), Eddy activity in the Lee of the Hawaiian Islands, *Deep Sea Res. Part II*, *55*, 1179–1194.
- Carton, J. A., G. Chepurin, X. Cao, and B. Giese (2000a), A simple ocean data assimilation analysis of the global upper ocean 1950–95. Part I: Methodology, *J. Phys. Ocean.*, *30*, 294–309.
- Carton, J. A., G. Chepurin, and X. Cao (2000b), A simple ocean data assimilation analysis of the global upper ocean 1950–95. Part II: Results, *J. Phys. Ocean.*, *30*, 311–326.
- Chaigneau, A., A. Gizolmea, and C. Gradosb (2008), Mesoscale eddies off Peru in altimeter records: Identification algorithms and eddy spatio-temporal patterns, *Prog. Oceanogr.*, *79*, 106–119, doi:10.1016/j.pocan.2008.10.013.
- Chavanne, C., P. Flament, R. Lumpkin, B. Dousset, and A. Bentamy (2002), Scatterometer observations of wind variations by oceanic islands: Implications for wind driven ocean circulation, *J. Remote Sens.*, *28*, 466–474.
- Chelton, D. B., M. G. Schlax, R. Samelson, and R. A. de Szoeke (2007), Global observations of large oceanic eddies, *Geophys. Res. Lett.*, *34*, L15606, doi:10.1029/2007GL030812.
- Clark, D. K., H. R. Gordon, K. J. Voss, Y. Ge, W. Broenkow, and C. Trees (1997), Validation of atmospheric correction over the oceans, *J. Geophys. Res.*, *102*, 17,209–17,217.
- Clark, D. K., M. A. Yarbrough, M. E. Feinholz, S. Flora, W. Broenkow, Y. S. Kim, B. C. Johnson, S. W. Brown, M. Yuen, and J. L. Mueller (2003), MOBY, a radiometric buoy for performance monitoring and vicarious calibration of satellite ocean color sensors: Measurement and data analysis protocols, in *Ocean Optics Protocols for Satellite Ocean Color Sensor Validation, 4th ed., Special Topics in Ocean Optics Protocols and Appendices*, vol. VI, edited by J. L. Mueller, G. S. Fargion, and C. R. McClain, pp. 3–34, NASA Goddard Space Flight Cent., Greenbelt, Md.
- Cushman-Roisin, B. (1994), *Introduction to Geophysical Fluid Dynamics*, 320 pp., Prentice Hall, Englewood Cliffs, N. J.
- Dickey, T. D., and R. R. Bidigare (2005), Interdisciplinary oceanographic observations: The wave of the future, *Sci. Mar.*, *69*, suppl. 1, 23–42.
- Dickey, T. D., F. Nencioli, V. S. Kuwahara, C. Leonard, W. Black, Y. M. Rii, R. R. Bidigare, and Q. Zhang (2008), Physical and biological observations of oceanic cyclones west of the island of Hawai'i, *Deep Sea Res. Part II*, *55*, 1195–1217.
- Doglioli, A. M., B. Blanke, S. Speich, and G. Lapeyre (2007), Tracking coherent structures in regional ocean model with wavelet analysis: Application to Cape Basin eddies, *J. Geophys. Res.*, *112*, C05043, doi:10.1029/2006JC003952.
- Dong, C., and J. C. McWilliams (2007), A numerical study of island wakes in the Southern California Bight, *Cont. Shelf Res.*, *27*, 1233–1248, doi:10.1016/j.csr.2007.01.016.
- Dong, C., J. C. McWilliams, and A. F. Shchepetkin (2007), Island wakes in deep water, *J. Phys. Ocean.*, *37*, 962–981, doi:10.1175/JPO3047.1.
- Dong, C., E. Idica, and J. McWilliams (2009), Circulation and multiple-scale variability in the Southern California Bight, *Prog. Oceanogr.*, doi:10.1016/j.pocan.2009.07.005, in press.
- Isern-Fontanet, J., E. Garcia-Ladona, and J. Font (2003), Identification of marine eddies from altimetric maps, *J. Atmos. Oceanic Technol.*, *20*, 772–778.
- Jimenez, B., P. Sangra, and E. Mason (2008), A numerical study of the relative importance of wind and topographic forcing on oceanic eddy shedding by tall, deep water islands, *Ocean Modell.*, *22*, 146–157.
- Jin, X., C. Dong, J. Kurian, J. McWilliams, D. Chelton, and Z. Li (2009), Wind-SST interaction in coastal upwelling: oceanic simulation with an empirical coupling, *J. Phys. Oceanogr.*, in press.
- Kuwahara, V. S., F. Nencioli, T. D. Dickey, Y. M. Rii, and R. R. Bidigare (2008), Physical dynamics and biological implications of Cyclone Noah in the lee of Hawai'i during E-Flux I, *Deep Sea Res. Part II*, *55*, 1231–1251.
- Landry, M. R., M. Decima, M. P. Simmons, C. C. S. Hannides, and E. Daniels (2008), Mesozooplankton biomass and grazing responses to Cyclone Opla, *Deep Sea Res. Part II*, *55*, 1378–1388.
- Lankhorst, M. (2006), A self-contained identification scheme for eddies in drifter and float trajectories, *J. Atmos. Oceanic Technol.*, *23*, 1583–1592, doi:10.1175/JTECH1931.1.
- LeBlond, P., and L. A. Mysak (1978), *Waves in the Ocean*, 602 pp., Elsevier, Amsterdam, Netherlands.
- Lilly, J. M., and J.-C. Gascard (2006), Wavelet ridge diagnosis of time-varying elliptical signals with application to an oceanic eddy, *Nonlinear Processes Geophys.*, *13*, 467–483.
- Lumpkin, C. F. (1998), Eddies and currents in the Hawaiian islands, Ph.D. dissertation, 281 pp., Univ. of Hawaii at Manoa, Manoa, Hawaii.
- Lumpkin, R., and Z. Garraffo (2005), Evaluating the decomposition of tropical Atlantic drifter observations, *J. Atmos. Oceanic Technol.*, *22*, 1403–1415.
- Lumpkin, R., and M. Pazos (2007), Measuring surface currents with Surface Velocity Program drifters: The instrument, its data, and some recent results, in *Lagrangian Analysis and Prediction of Coastal and Ocean Dynamics*, edited by A. Griffa et al., chap. 2, pp., Cambridge Univ. Press, Cambridge, U. K.

- Nencioli, F., T. D. Dickey, V. S. Kuwahara, R. R. Bidigare, and Y. M. Rii (2008), Physical dynamics and biological implications of a mesoscale eddy in the lee of Hawaii: Cyclone Opal observations during E-Flux III, *Deep Sea Res. Part II*, *55*, 1195–1217.
- Patzert, W. C. (1969), Eddies in Hawaiian Islands, *Rep. HIG-69-8*, Hawaii Inst. of Geophys., Manoa, Hawaii.
- Pullen, J., J. D. Doyle, P. May, C. Chavanne, P. Flament, and R. A. Arnone (2008), Monsoon surges trigger oceanic eddy formation and propagation in the lee of the Philippine islands, *Geophys. Res. Lett.*, *35*, L07604, doi:10.1029/2007GL033109.
- Qiu, B., D. A. Koh, C. Lumpkin, and P. Flament (1997), Existence and formation mechanism of the north Hawaiian ridge current, *J. Phys. Oceanogr.*, *27*, 431–444.
- Rii, Y. M., S. L. Brown, F. Nencioli, V. Kuwahara, T. Dickey, D. M. Karl, and R. R. Bidigare (2008), The transient oasis: Nutrient-phytoplankton dynamics and particle export in Hawaiian lee cyclones, *Deep Sea Res. Part II*, *55*, 1275–1290.
- Sadarjoen, A., and F. H. Post (2000), Detection, quantification, and tracking of vortices using streamline geometry, *Visual. Comput. Graphics*, *24*, 333–341.
- Sangra, P., M. Auladellb, A. Marrero-Diaza, J. L. Pelegrib, E. Fraile-Nueza, A. Rodriguez-Santanaa, J. M. Martin, E. Masona, and A. Hernandez-Guerraa (2007), On the nature of oceanic eddies shed by the Island of Gran Canaria, *Deep Sea Res. Part I*, *54*, 687–709.
- Seki, M. P., J. J. Polovina, R. E. Brainard, R. R. Bidigare, C. L. Leonard, and D. G. Foley (2001), Biological enhancement at cyclonic eddies tracked with GOES thermal imagery in Hawaiian waters, *Geophys. Res. Lett.*, *28*, 1583–1586.
- Seki, M. P., R. Lumpkin, and P. Flament (2002), Hawaii cyclonic eddies and blue marlin catches: the case study of the 1995 Hawaiian International Billfish Tournament, *J. Oceanogr.*, *58*, 739–745.
- Shchepetkin, A. F., and J. C. McWilliams (2005), The Regional Oceanic Modeling System (ROMS): A split-explicit, free-surface, topography-following-coordinate oceanic model, *Ocean Modell.*, *9*, 347–404, doi:10.1016/j.ocemod.2004.08.002.
- Siegel, A., and J. B. Weiss (1997), A wavelet-packet census algorithm for calculating vortex statistics, *Phys. Fluids*, *9*, 1988–1999.
- Signell, R. P., and W. R. Geyer (1991), Transient eddy formation around headlands, *J. Geophys. Res.*, *96*, 2561–2575.
- Tolman, H. L. (2002), User manual and system documentation of WAVEWATCH-III version 2.22, *Tech. Note 222*, 133 pp., NOAA, Washington, D. C.
- Vaillancourt, R. D., J. Marra, M. P. Seki, M. L. Parsons, and R. R. Bidigare (2003), Impact of a cyclonic eddy field on phytoplankton community structure and photosynthetic competency in the subtropical North Pacific Ocean, *Deep Sea Res. Part I*, *50*, 829–847.
- Zhang, H.-M., J. J. Bates, and R. W. Reynolds (2006), Assessment of composite global sampling: Sea surface wind speed, *Geophys. Res. Lett.*, *33*, L17714, doi:10.1029/2006GL027086.

D. K. Clark, T. Mavor, and M. Ondrusek, STAR, NESDIS, NOAA, 5200 Auth Road, Camp Springs, MD 20746, USA.

T. Dickey, S. Jiang, and F. Nencioli, Department of Geography, University of California, 1832 Ellison Hall, Santa Barbara, CA 93016-4060, USA.

C. Dong, J. C. McWilliams, and Y. Uchiyama, Institute of Geophysics and Planetary Physics, University of California, 405 Hilgard Avenue, Los Angeles, CA 90095-1567, USA. (cdong@atmos.ucla.edu)

H. Zhang, Jet Propulsion Laboratory, California Institute of Technology, 4800 Oak Grove Drive, Mail Stop 300-324, Pasadena, CA 91109, USA.